Activated carbon from *Thapsia transtagana* stems: central composite design (CCD) optimization of the preparation conditions and efficient dyes removal

A. Machrouhi[a], M. Farnane[a], H. Tounsadi[b], Y. Kadmi[c], L. Favier[d],
S. Qourzal[e], M. Abdennouri[a], N. Barka[a,*]

[a]*Sultan Moulay Slimane University of Beni Mellal, Research Group in Environmental Sciences and Applied Materials (SEMA), FP Khouribga, B.P. 145, 25000 Khouribga, Morocco, Tel. +212 661 66 66 22; Fax: +212 523 49 03 54; email: barkanoureddine@yahoo.fr (N. Barka), Tel. +21251039586; email: machrouhi.aicha90@gmail.com (A. Machrouhi), Tel. +212667669039; email: abdennourimohamed@yahoo.fr (M. Abdennouri)*
[b]*Laboratoire d'Ingénierie, d'Electrochimie, de Modélisation et d'Environnement, Université Sidi Mohamed Ben Abdellah, Faculté des Sciences Dhar El Mahraz, Fès, Morocco, Tel. +21245208564; email: hananetounsadi@gmail.com*
[c]*Université de Lille, LASIR; UMR CNRS 8516, Villeneuve d'Ascq, France, Tel. +33321603700; email: yassine.kadmi@gmail.com*
[d]*Ecole Nationale Supérieure de Chimie de Rennes, CNRS, UMR 6226, 11 Allée de Beaulieu, CS 50837, 35708 Rennes Cedex 7, France, Tel. +33223238135; email: lidia.favier@ensc-rennes.fr*
[e]*Equipe de Catalyse et Environnement, Département de Chimie, Faculté des Sciences, Université Ibn Zohr, B.P. 8106 Cité Dakhla, Agadir, Morocco, Tel. +212662896006; email: samir_qourzal@yahoo.fr*

Received 21 January 2019; Accepted 24 May 2019

ABSTRACT

This study investigates the preparation of activated carbons from *Thapsia transtagana* stems using chemical H_3PO_4 activation and their ability for cationic and anionic dyes removal from aqueous solution. Central composite design and response surface methodology (RSM) were used for the optimization of the preparation conditions and dyes removal efficiency. Five responses were targeted which are iodine number (IN), methylene blue index (MB index) and removal efficiency for methyl violet (MV), methyl orange (MO) and indigo carmine (IC). From the experimental results, the maximum iodine number and methylene blue index obtained were 1,082.22 and 397.54 mg g^{-1}, respectively. The highest removal efficiency for methyl violet was obtained by activated carbon sample activated at 400°C for 145 min with an impregnation ratio of 2 g g^{-1}. For methyl orange, the best conditions were activation temperature of 450°C, impregnation ratio of 1.5 g g^{-1} and activation time of 155 min. For indigo carmine, activation temperature of 500°C, impregnation ratio of 2 g g^{-1} and activation time of 145 min. Under these conditions, the maximum adsorption capacities were 358.68 mg g^{-1} for methyl violet, 305.88 mg g^{-1} for methyl orange and 196.06 mg g^{-1} for indigo carmine. The best activated carbon samples were characterized by Fourier transform infrared spectroscopy, XRD and scanning electron microscopy–energy-dispersive X-ray. The functional groups were also determined by Boehm titration.

Keywords: Activated carbon; *Thapsia transtagana*; Dyes removal; Central composite design

1. Introduction

The presence of dyes in effluents is a major concern due to their adverse effect to many forms of life. The discharge of dyes in the environment is worrying for both toxicological and esthetical reasons [1]. Dyes are an important class of pollutants which came in large amounts from textile, dyeing, paper and pulp, and tannery and paint industries [2]. It is

* Corresponding author.

already demonstrated that the industrial effluents containing dyes reduce light penetration, preventing the photosynthesis of aqueous flora [3]. Moreover, many dyes are toxic and even carcinogenic thus affecting the aquatic biota and human health [4–6].

Many technologies are employed to achieve the regulatory standard for treated water discharge such as sorption, coagulation/flocculation, chemical oxidation, membrane separation, electrochemical, aerobic and anaerobic microbial degradation. From all these processes, adsorption is a preferred method due to its low cost and effectiveness [7–10]. Also, adsorption removes the entire dye molecule, leaving no fragments in the effluent. In adsorption process, activated carbon is the most generally used adsorbent for dye removal from effluent [11], due to its high efficiency. For economic reasons, many low cost and abundant biomaterials were tested as sorbents in their native form or after activation, such as avocado kernels seeds and *Ziziphus lotus* fruit peels [12], *Thapsia transtagana* stems (TTS) [13], *prosopis africana* seed hulls [14], pecan shell [15], *Elaeagnus angustifolia* L. fruits [16], orange peel [17], bamboo [18], rattan sawdust [19], rice husk [20], waste tea [21], *Acacia mangium* wood [22], date stones [23] and banana waste [24].

Generally, activation of precursor can be carried out either through physical or chemical activation method. Physical activation involves the carbonization of the raw materials under inert atmosphere followed by the activation of the resulting char at high temperature in the presence of carbon dioxide or steam. This process has several drawbacks represented in the low carbon yield and high energy consumption [25]. While, in chemical activation, the precursor material is impregnated with activating agents such as potassium hydroxide (KOH) [26], zinc chloride (ZnCl$_2$) [27], phosphoric acid (H$_3$PO$_4$) [28], potassium carbonate (K$_2$CO$_3$) [29], etc. Thereafter, the impregnated material is subjected to heat treatment in an inert atmosphere. These chemical agents have dehydrating properties that influence the pyrolytic decomposition and prevent the formation of tars and volatile organic compounds during activation at high temperature producing high efficiency activated carbon.

Indeed, the H$_3$PO$_4$ activation mechanisms are identified and published on this subject reveals a dual activation mode [30]. First, phosphoric acid acts as an acid catalyst that promotes depolymerization of the macromolecules making up the biomass (cellulose, hemicellulose and lignin) whereas encouraging the formation of cross-linking through dehydration, cyclization and condensation reactions. Second, H$_3$PO$_4$ is known to promote the formation of phosphate and polyphosphate bridges that connect and cross-link the fragments derived from the macromolecules making up the biomass [31]. This means that the insertion of phosphate groups leads to a dilation process, which, after elimination of the acid, leaves a matrix in a developed state with an accessible porous structure.

The production of activated carbons with high yield, large surface area and suitable pore size depends upon the production conditions [32]. These conditions must be properly balanced in order to obtain activated carbons with desirable properties. The main factors of the preparation method that influence the properties of activated carbons are impregnation ratio; activation temperature and

activation time [33,34]. The best operating conditions for the production of activated carbon can be evaluated by the use of a sufficient experimental design. Response surface methodology (RSM) is a set of statistical and mathematical techniques used for designing experiment, response surface modeling through regression, evaluating the effects of several factors and searching optimum conditions for desirable responses and reducing number of experiments [35].

The objective of this study was the utilization of TTS biomass as a new precursor for highly efficient activated carbons by phosphoric acid activation and their evaluation for both cationic and anionic dyes removal. Central composite design (CCD) combined with RSM was used to decrease in the number of experimental runs. The conditions optimized were impregnation ratio, activation temperature and activation time. Five responses were targeted which are iodine number (IN), methylene blue index (MB index) and removal efficiency for methyl violet (MV), methyl orange (MO) and indigo carmine (IC). The ACs produced at the optimal conditions were characterized by Fourier transform infrared spectroscopy (FTIR), XRD, scanning electron microscopy–energy-dispersive X-ray (SEM-EDX) and the point of zero charge (pH$_{PZC}$). The functional groups were also determined by Boehm titration.

2. Material and methods

2.1. Material

All the chemicals/reagents used in this study were of analytical grade. H$_3$PO$_4$ (85%), HCl (37%), I$_2$ (99.8%–100.5%), Na$_2$S$_2$O$_3$5H$_2$O, Na$_2$CO$_3$, NaHCO$_3$ (99.5%–100.5%), commercial activated carbon (powder form) (100%), methyl violet, methyl orange and indigo carmine were purchased from Sigma-Aldrich (Germany) (100%). Methylene blue was purchased from Panreac (Spain) (100%). HNO$_3$ (65%) was provided from Scharlau (Spain). NaOH (≥99%) from Merck (Germany), potassium iodide (KI) (100%) was obtained from Pharmac (Morocco). The characteristics and chemical structure of the dyes are listed in Table 1.

2.2. Preparation of activated carbons

The TTS were used as precursor for the preparation of activated carbon. They were cut into small pieces and powdered to a particle size less than 125 μm using a domestic mixer. 15 g of the biomass were impregnated with H$_3$PO$_4$ as the activating agent at desired mass ratio. The samples were heated at 105°C for 24 h to remove excess moisture and loaded in a stainless steel vertical tubular reactor placed into a furnace under purified nitrogen atmosphere. After activation at desired temperature during desired time, the residual phosphoric acid was eliminated from the activated carbons by deionized water. The obtained powder was then dried at 105°C, powdered, sieved using a normalized sieve and stored in hermetic bottle for further tests.

The method of calculating the volume of H$_3$PO$_4$ is:

$$V_{H_3PO_4} = \frac{\left(\dfrac{m\left(H_3PO_4\right)}{P} \times 100 \right)}{d} \tag{1}$$

Table 1
Molecular structure and physical characteristics of the dyes

Dye name	Generic name	Molecular structure	λ_{max} (nm)	Mw (g mol^{-1})
Methyl violet (MV)	Basic violet 1		584	393.95
Methylene blue (MB)	Basic blue 9		663	319.85
Methyl orange (MO)	Acid orange 52		465	327.33
Indigo carmine (IC)	Acid blue 74		610	466.36
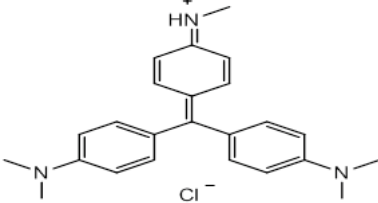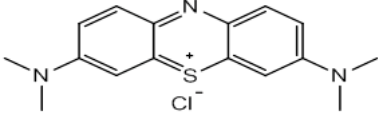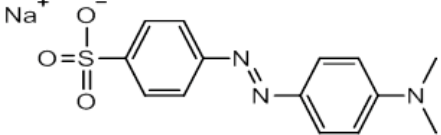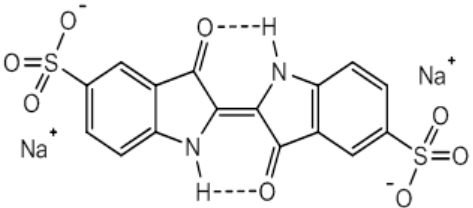
The impregnation ratio of the activating agent with the precursor was computed using Eq. (1):

$$\text{Impregnation ratio} = \left(\frac{\text{dried weight of H}_3\text{PO}_4}{\text{mass of the precursor (TTS)}} \right) \quad (2)$$

2.3. Design of experiments using central composite design

CCD was used to study the individual and synergetic effect of the three factors toward defined responses. This method can reduce the number of experimental trials required to evaluate main effect of each parameter and their interactions [36]. It is characterized by three operations namely: 2^n factorial runs, $2n$ axial runs and six center runs [37]. For this case, it translated into eight factorial points, six axial points and six replicates at the center which gives a total of 20 experiments as calculated from Eq. (2):

$$\text{Total number of experiments } (N) \; = \; 2^n + 2n + \text{nc} \quad (3)$$

where n is the number of factors, nc is the number of center points (six replicates).

The two-level independent variables were coded as +1 and –1 for high and low values, respectively, and were used to represent the eight factorial points. The six axial points were located at $(\pm\alpha, 0, 0)$, $(0, \pm\alpha, 0)$, $(0, 0, \pm\alpha)$, and the six replicates were at the center $(0, 0, 0)$ [38]. Alpha (α) approximately show the distance of the axial from center point, which is rotatable

and strongly depends on the number of factorial points and can be calculated from Eq. (3) [39]:

$$\alpha = N_p^{1/4} \quad (4)$$

In this study, the independent variables studied were activation temperature (A), impregnation ratio (B) and activation time (C). These three variables with their respective ranges were selected based on the literature and preliminary studies as given in Table 2 [40].

The optimal conditions for the studied responses which are iodine number, methylene blue index and removal efficiencies for methyl violet, methyl orange and indigo carmine were determined using the quadratic model given by Eq. (4) [41]:

$$Y = b_0 + \sum_{i=1}^{n} b_i X_i + \left(\sum_{i=1}^{n} b_{ii} X_i \right)^2 + \sum_{i=1}^{n-1} \sum_{j=i+1}^{n} b_{ii} X_i X_j \quad (5)$$

where Y is the predicted response, b_0 is the constant coefficients, b_{ii} is the quadratic coefficient, b_{ij} is the interaction coefficient and x_i, x_j are the coded values of the considered variables.

The quality of the fit to the polynomial model was expressed by the correlation coefficient (R^2). The significance and adequacy of the used model was further explained using F-value (Fisher variation ratio), probability value (Prob > F) and adequate precision (AP) [41].

Table 2
Process factors and their levels

Variable	Code	Coded variable levels				
		$-\alpha$	-1	0	1	$+\alpha$
Activation temperature, °C	A	366	400	450	500	534
Impregnation ratio, g g⁻¹	B	0.66	1	1.5	2	2.34
Activation time, min	C	105	115	130	145	155

2.4. Evaluation of activated carbons

2.4.1. Iodine number (IN)

It is a simple and commonly used technique for the rapid assessment of activated carbons quality. It is a measure of micropore content of the activated carbon (0–2 nm) by adsorption of iodine from solution. The iodine number values expected for good quality AC to be equal to or higher than 900 mg g⁻¹. It has been also reported that the typical I_2 number range is 500–1,200 mg g⁻¹ which is equivalent to the surface area between 900 and 1,100 m² g⁻¹ [42]. The iodine number is defined as the milligrams of iodine adsorbed by 1.0 g of carbon when the iodine concentration of the filtrate is 0.02 N. It was determined according to the ASTM D4607-94 method [43]. 1 g of each ACs is treated with 10.0 mL of 5% HCl and boiled for 30 s and subsequently cooled. About 100 mL of 0.1 N iodine solutions was added to the mixture and stirred for 30 min. The resulting solution was filtered and 50 mL of the filtrate was titrated with 0.1 N sodium thiosulfate using starch as indicator.

2.4.2. Methylene blue index (MB index)

The methylene blue index is a measure of mesoporosity (2–50 nm) present in activated carbon. It is defined as the maximum amount of dye adsorbed on 1.0 g of adsorbent. To have maximum sorption capacities of methylene blue onto ACs, the adsorption isotherms were investigated. Stock solution of methylene blue was prepared by dissolving desired weight in distilled water. Sorption experiments were investigated in a series of beakers containing 100 mL by adding 100 mg of each ACs. Sorption equilibrium was established for different methylene blue initial concentration between 20 and 500 mg L⁻¹ at initial solution pH of 6.5 and room temperature. Residual concentrations were determined by spectrophotometric method at the wavelength of maximum absorbance of 663 nm.

2.4.3. Dyes removal efficiency

The dye solutions of methyl violet, methyl orange and indigo carmine at a concentration of 500 mg L⁻¹ were prepared by dissolving desired weight of each dye in distilled water. Sorption experiments were investigated at room temperature in a series of beakers containing 50 mL of the dyes solution at a concentration of 500 mg L⁻¹ and 50 mg of each activated carbon and commercial activated carbon. The mixtures were stirred for 2 h. After each sorption experiment, samples were centrifuged at 3,400 rpm for 10 min. The residual concentration was determined using UV–Vis spectrophotometer.

The adsorption capacity of the dyes at equilibrium was defined as the amount of adsorbate per gram of adsorbent (in mg g⁻¹) and was calculated using the following equation:

$$q = \frac{(C_0 - C)}{R} \tag{6}$$

where q is the adsorbed quantity (mg g⁻¹), C_0 is the initial dye concentration (mg L⁻¹), C is the residual dye concentration (mg L⁻¹) and R is the mass of activated carbon per liter of aqueous solution (g L⁻¹).

Adsorption isotherms were carried out by adding 0.05 g of activated carbons into a number of beakers containing 50 mL at different initial concentrations (100–500 mg L⁻¹) of dye solution at initial pH and room temperature. Equilibrium data obtained were analyzed using Langmuir and Freundlich isotherm models.

The Langmuir isotherm model is represented as follows:

$$q_e = \frac{q_m K_L C_e}{1 + K_L C_e} \tag{7}$$

where q_m (mg g⁻¹) is the maximum monolayer adsorption capacity, K_L (L mg⁻¹) is the Langmuir equilibrium constant related to the adsorption affinity and C_e is the equilibrium concentration.

The Freundlich equation can be stated as follows:

$$q_e = K_F C_e^{1/n} \tag{8}$$

where K_F (mg¹⁻¹ᐟⁿ g⁻¹ L¹ᐟⁿ) is the Freundlich constant and n is the heterogeneity factor. The K_F value is related to the adsorption capacity; while $1/n$ value is related to the adsorption intensity.

2.5. Surface and chemical characterization

The surface morphology of precursor material and optimized activated carbon was observed by SEM. Measurements were obtained with VEGA3-EDAX (TESCAN, Czech) equipped with an EDX. Small amount of each sample was finely powdered and mounted directly onto aluminum sample holder using two-sided adhesive carbon model. The functional groups present on the surface of activated carbon were determined by FTIR (FTIR-2000, PerkinElmer, USA). The infrared spectra of the starting material and activated carbons were collected in a range of 4,000–400 cm⁻¹. The XRD measurements were performed at room temperature on a D2 Phaser diffractometer, with the Bragg–Brentano

geometry, using CuKα target (λ = 1.5406 Å) operated at 30 kV and 10 mA. The XRD scans were recorded in the 2θ range 10°–80° with step size 0.01° (0.5 s/step). The acidic and basic functional groups on the surface of ACs were determined quantitatively by the Boehm's titration method [44]. About 0.1 g of each sample was mixed with 50 mL of 0.01 M aqueous reactant solution (NaOH, Na_2CO_3, $NaHCO_3$ or HCl). The mixtures were stirred at 500 rpm for 24 h at room temperature. Then, the suspensions were filtrated by a 0.45 μm membrane filter. To determine the oxygenated groups, back titrations of the filtrate (10 mL) were achieved with standard 0.01 M HCl solution. Basic groups were also determined by back titration of the filtrate with 0.01 M NaOH solution. The point of zero charge (pH_{PZC}) was determined by the pH drift method according to the method proposed by Noh and Schwarz [45]. The pH of NaCl aqueous solution (50 mL at 0.01 mol L^{-1}) was adjusted to successive initial values in the range of 2–12 by addition of HNO_3 and/or NaOH. Moreover, 0.05 g of each adsorbent was added in the solution and stirred for 6 h. The final pH was measured and plotted vs. the initial pH. The pH_{PZC} was determined at the value for which pHfinal = pHinitial.

3. Results and discussion

3.1. Experimental results

This study investigates the relationship between five responses (iodine number (Y_1), methylene blue index (Y_2), adsorption capacity of methyl orange (Y_3), adsorption capacity of methyl violet (Y_4) and adsorption capacity of indigo carmine (Y_5)) and three independent factors (activation temperature (A), impregnation ratio (B) and activation time (C)). Table 3 shows the preparation conditions and the experimental results for the five responses. From the table, it could be seen that the adsorption capacity of dyes was influenced by the three factors. The best conditions for the removal of methyl violet were obtained by activated carbon sample activated at 400°C for 145 min with an impregnation ratio of 2 g g^{-1}. For methyl orange, the best conditions were activation temperature of 450°C, impregnation ratio of 1.5 g g^{-1} and activation time of 155 min. For indigo carmine, activation temperature of 500°C, impregnation ratio of 2 g g^{-1} and activation time of 145 min. Under these conditions, the maximum sorption capacities were 358.67 mg g^{-1} for methyl violet, 305.88 mg g^{-1} for methyl orange and 196.06 mg g^{-1} for indigo carmine. The methylene blue index varied between 237.59 and 397.54 mg g^{-1}, which indicated a great mesoporosity for all activated carbon samples. The greater iodine number of 1,082.22 mg g^{-1} is obtained for the activated carbon activated at 500°C for 115 min with an impregnation ratio of 2 g g^{-1}.

Moreover, regression analysis was performed to fit the response functions with the experimental data. The values of regression coefficient obtained are illustrated in Table 4. From this table, it can be seen that the regression coefficients for the impregnation ratio factor are higher than those of the other factors. Also, there is an increase in the

Table 3
Experimental design matrix coded, real values and experimental results for the responses

Run	Activation temperature (°C)		Impregnation ratio (g g^{-1})		Activation time (min)		Responses (mg g^{-1})				
	Coded	Actual	Coded	Actual	Coded	Actual	Iodine number	Methylene blue index	Methyl orange	Methyl violet	Indigo carmine
1	0	450	0	1.5	0	130	1,019.39	307.21	270.35	311.93	159.32
2	0	450	0	1.5	0	130	1,015.20	302.36	266.15	311.37	157.74
3	1	500	−1	1	−1	115	976.11	258.17	246.45	239.86	149.34
4	0	450	0	1.5	1.682	155	1,038.94	318.40	305.88	349.66	188.97
5	0	450	0	1.5	−1.682	105	1,004.03	313.26	260.66	304.89	149.87
6	−1	400	−1	1	1	145	1,029.16	313.50	253.56	239.58	136.48
7	0	450	0	1.5	0	130	1,023.58	310.43	262.60	313.34	154.07
8	−1.682	366	0	1.5	0	130	1,031.96	284.51	255.82	291.66	128.61
9	1	500	1	2	−1	115	1,082.22	317.48	295.89	338.68	176.64
10	−1	400	−1	1	−1	115	1,001.24	293.25	246.77	217.90	117.32
11	0	450	0	1.5	0	130	1,012.41	305.99	269.71	307.99	158.79
12	0	450	−1.682	0.66	0	130	997.05	237.59	205.43	101.34	76.64
13	1	500	−1	1	1	145	948.19	245.16	239.99	206.64	130.97
14	−1	400	1	2	1	145	1,045.92	397.54	287.47	358.68	164.57
15	1	500	1	2	1	145	1,059.88	339.57	289.09	352.47	196.06
16	−1	400	1	2	−1	115	990.07	339.59	270.67	317.00	131.49
17	0	450	0	1.5	0	130	1,011.01	306.13	268.74	304.33	160.37
18	0	450	1.682	2.34	0	130	1,048.71	357.97	303.94	337.55	148.55
19	0	450	0	1.5	0	130	1,018.00	305.69	265.51	310.53	155.64
20	1.682	534	0	1.5	0	130	1,066.86	302.15	302.65	300.95	169.55

Table 4
Values of model coefficients for the five responses

Main coefficients	Y_1	Y_2	Y_3	Y_4	Y_5
b_0	1,017.16	305.91	267.41	309.75	157.38
b_1	4.29	−11.26	6.71	1.47	12.59
b_2	22.71	35.61	23.56	62.94	18.70
b_3	6.70	7.01	6.26	8.67	8.66
b_{12}	26.47	2.91	5.08	3.30	6.25
b_{13}	−16.59	−8.55	−4.56	−10.25	−6.33
b_{23}	4.15	9.01	1.20	8.29	6.40
b_{11}	8.31	−2.28	2.88	−3.85	−1.46
b_{22}	−1.07	−0.71	−5.80	−31.02	−14.35
b_{33}	−1.61	5.71	4.28	7.12	5.76

adsorption capacities with the increase of the impregnation ratio. Therefore, we can conclude that the most influencing factor on the five responses was the impregnation ratio. The activation temperature has a negative effect on methylene blue index, however, it presented a positive effect on iodine number, methyl orange, methyl violet and indigo carmine removal. While, the increase in the impregnation ratio and activation time enhanced the five responses.

3.2. Analysis of variance

The analysis of variance ANOVA was performed for adequacy and significance of predicted model. After discarding the insignificant terms, the ANOVA data for the coded quadratic models for the five responses at a confidence level of 95% are represented in Tables 5a–e. The effect of a factor is defined as the change in the response produced by a change in the level of the factor. This is frequently called a main effect because it refers to the primary factors of interest in the experiment. The ANOVA results showed that the equations adequately represented the actual relationship between each response and the significant variables. The F-value implies that the models are significant and values of "Prob > F" less than 0.05 indicate that models terms are significant. Especially larger F-value with the associated p-value (smaller than 0.05, confidence interval) means that the experimental systems can be modeled effectively with less error. Therefore, interaction effects as adequate model terms can be used for modeling the experimental system.

3.2.1. Iodine number

According to the ANOVA for the iodine number, the significant model factors are the activation temperature (A), impregnation ratio (B), activation time (C), the interaction between activation temperature and impregnation ratio (AB), the interaction between activation temperature and activation time (AC) and the quadratic term of activation temperature (A^2) (Eq. (6)).

$$Y_1 = 1,015.16 + 4.29\ A + 22.71\ B + 6.70\ C + 26.47\ AB - 16.59\ AC + 8.54\ A^2 \tag{9}$$

The activation temperature, the impregnation ratio, the activation time, the interaction between activation temperature, impregnation ratio and the quadratic term of activation temperature showed a positive effect on the iodine number. Although, the interaction between activation temperature and activation time showed a negative effect on the iodine number, the impregnation ratio has the largest significant effect on the iodine number due to the high F-value (42.82) followed by the interaction between activation temperature and impregnation ratio, the interaction between activation temperature and activation time and the quadratic term of activation temperature with an F-value of 34.19, 13.64 and 6.51, respectively. Hence, it could be seen that the number of micropores are higher with the impregnation ratio of 2 g g^{-1} in the studied domain. In fact, at high level of the significant model terms, the activation reaction may take place rapidly producing a development of the porosity of the obtained activated carbons, and moreover, an increase in the microporosity.

For the iodine number, the most significant interactions were the interaction between activation temperature and impregnation ratio and the interaction between activation temperature and activation time. It could be seen from Fig. 1a that the iodine number increased with increasing activation temperature and impregnation ratio when the activation time is fixed at 115 min. Fig. 1b shows that the iodine number increased with increasing activation temperature and decreasing activation time when the impregnation ratio is fixed at 2 g g^{-1}.

3.2.2. Methylene blue index

For methylene blue index, the most significant effects are activation temperature (A), impregnation ratio (B), activation time (C), interaction between activation temperature and impregnation ratio (AB) and the interaction between impregnation ratio and activation time (BC) and the quadratic term of activation time (C^2) Eq. (7).

$$Y_2 = 303.68 - 11.26\ A + 35.61\ B + 7.01\ C + 2.91\ AB + 9.01\ BC + 5.96\ C^2 \tag{10}$$

The impregnation ratio and activation time and interaction effects between activation temperature and impregnation

Table 5a
ANOVA results of the response surface quadratic model for iodine number

Source	Sum of squares	Degree of freedom	Mean square	F-value	p-value Prob > F	Lack of fit	Comment
Model	16,870.08	6	2,811.68	17.08	0.00002	11.62	Significant
A	252.03	1	252.03	1.53	0.23791		
B	7,051.10	1	7,051.10	42.82	0.00002		
C	620.24	1	620.24	3.77	0.07428		
AB	5,629.14	1	5,629.14	34.19	0.00006		
AC	2,245.51	1	2,245.51	13.64	0.00271		
A^2	1,072.07	1	1,072.07	6.51	0.02412		
Residual	2,140.60	13	164.66				
Corrected total	19,010.67	19					

$R^2 = 0.8874$; $R^2_{adj} = 0.8354$.

Table 5b
ANOVA results of the response surface quadratic model for methylene blue index

Source	Sum of squares	Degree of freedom	Mean square	F-value	p-value Prob > F	Lack of fit	Comment
Model	21,003.08	6	3,500.51	11.36	0.00016	71.08	Significant
A	1,735.06	1	1,735.06	5.63	0.03374		
B	17,334.41	1	17,334.41	56.26	0.00001		
C	677.69	1	677.69	2.2	0.16188		
AB	68.1	1	68.1	0.22	0.64605		
BC	662.49	1	662.49	2.15	0.16632		
C^2	525.34	1	525.34	1.71	0.21426		
Residual	4,005.27	13	308.1				
Corrected total	25,008.35	19					

$R^2 = 0.8398$; $R^2_{adj} = 0.7659$.

Table 5c
ANOVA results of the response surface quadratic model for methyl orange removal

Source	Sum of squares	Degree of freedom	Mean square	F-value	p-value Prob > F	Lack of fit	Comment
Model	9,429.39	6	1,571.56	9.38	0.00042	30.53	Significant
A	615.27	1	615.27	3.67	0.07755		
B	7,592	1	7,591.1	45.32	0.00001		
C	541.54	1	541.54	3.23	0.09543		
AB	207.26	1	207.26	1.24	0.28615		
AC	169.69	1	169.69	1.01	0.33256		
C^2	303.63	1	303.63	1.81	0.2012		
Residual	2,177.64	13	167.51				
Corrected total	11,607.02	19					

$R^2 = 0.8702$; $R^2_{adj} = 0.7533$.

ratio, impregnation ratio and activation time and quadratic term of activation time showed a positive effect on the methylene blue index response. However, the activation temperature presented a negative effect on the development of mesopores. According to Table 5b, the impregnation ratio has the utmost effect on methylene blue index based on the highest F-value of 56.26 whereas activation temperature and activation time produced analogous impacts on this response with F-values of 5.63 and 2.20, respectively. The interaction effects between activation temperature and impregnation ratio, impregnation ratio and activation time and that of quadratic term of activation time were

Table 5d
ANOVA results of the response surface quadratic model for methyl violet removal

Source	Sum of squares	Degree of freedom	Mean square	F-value	p-value Prob > F	Lack of fit	Comment
Model	71,851.64	7	10,264.52	98.79	<0.00001	16.04	Significant
A	29.62	1	29.62	0.29	0.60318		
B	54,164.20	1	54,164.20	521.29	<0.00001		
C	1,036.71	1	1,036.71	9.98	0.00824		
AC	856.79	1	856.79	8.25	0.01405		
BC	561.31	1	561.31	5.40	0.03847		
B^2	13,689.91	1	13,689.91	131.75	<0.00001		
C^2	819.93	1	819.93	7.89	0.01578		
Residual	1,246.86	12	103.91				
Corrected total	73,098.50	19					

$R^2 = 0.9871$; $R^2_{adj} = 0.9754$.

Table 5e
ANOVA results of the response surface quadratic model for indigo carmine removal

Source	Sum of squares	Degree of freedom	Mean square	F-value	p-value Prob > F	Lack of fit	Comment
Model	12,339.77	7	1,762.82	27.26	<0.00001	12.75	Significant
A	2,166.63	1	2,166.63	33.5	0.00009		
B	4,782.96	1	4,782.96	73.95	<0.00001		
C	1,035.1	1	1,035.1	16	0.00176		
AC	327.45	1	327.45	5.06	0.04399		
BC	334.16	1	334.16	5.17	0.04221		
B^2	2,943.97	1	2,943.97	45.52	<0.00002		
C^2	509.96	1	509.96	7.89	0.01581		
Residual	776.11	12	64.68				
Corrected total	13,115.88	19					

$R^2 = 0.9408$; $R^2_{adj} = 0.9063$.
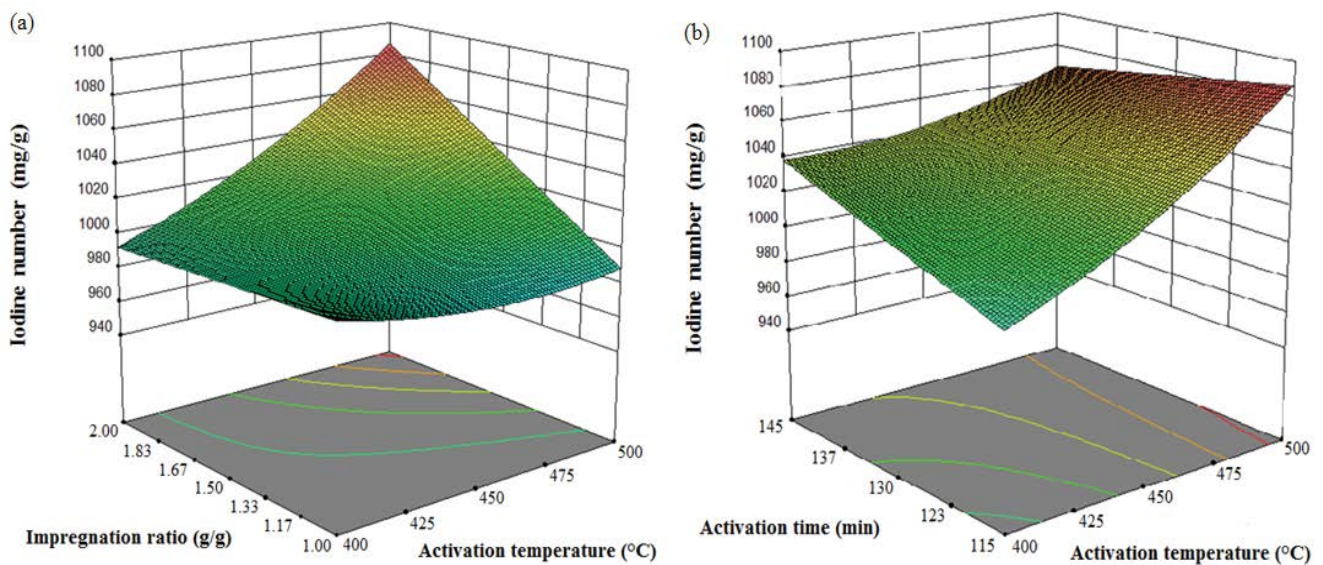
Fig. 1. Surface response plot for the iodine number: (a) interaction between impregnation ratio and activation temperature and (b) interaction between activation time and activation temperature.

slightly inconsequential with *F*-values of 0.22, 2.15 and 1.71, respectively.

The effect of interaction between activation temperature and impregnation ratio on methylene blue index can be observed by 3D response surface plot as shown in Fig. 2a. It can be seen from this figure that the methylene blue index increased with the decreasing of the activation temperature and the increase in impregnation ratio. A maximal methylene blue index response is obtained with an activation time of 145 min. Fig. 2b shows that when the impregnation ratio and activation time was increased, the methylene blue index also increases.

3.2.3. Methyl orange removal

The most significant effects for methyl orange removal response are activation temperature (*A*), impregnation ratio (*B*), activation time (*C*), the interaction between activation temperature and impregnation ratio (*AB*), the interaction between activation temperature and activation time (*AC*) and the quadratic term of activation time (*C*²) Eq. (8).

$$Y_3 = 265.24 + 6.71\ A + 23.56\ B + 6.26\ C + 5.08\ AB - $$
$$4.56\ AC + 4.53\ C^2 \tag{11}$$

Thus, all the term showed a positive effect on methyl orange removal except the interaction between activation temperature and activation time. It can clearly be seen from Table 5c that impregnation ratio has the utmost effect on methyl orange removal based on the highest *F*-value of 45.32. The other terms were slightly inconsequential. Therefore, the removal of methyl orange increased when impregnation ratio varied from low to high levels. Hence, high adsorption capacities of methyl orange were observed for activated carbons with high impregnation ratio.

From Fig. 3a it can be observed that the adsorption capacity for methyl orange increases with the increase in activation temperature as well as impregnation ratio. The methyl orange removal increased when the activation temperature

and activation time increased (Fig. 3b). The maximal methyl orange removal was obtained with an activation time of 145 min and an impregnation ratio of 2 g g⁻¹.

3.2.4. Methyl violet removal

The significant model terms for methyl violet removal are the activation temperature (*A*), impregnation ratio (*B*), activation time (*C*), the interaction between activation temperature and activation time (*AC*), the interaction between impregnation ratio and activation time (*BC*) and the quadratic terms of impregnation ratio (*B*²) and activation time (*C*²) (Eq. (9)).

$$Y_4 = 306.61 + 1.47\ A + 62.94\ B + 8.67\ C - 10.25\ AC + $$
$$8.29\ BC - 30.65\ B^2 + 7.47\ C^2 \tag{12}$$

The activation temperatures, the impregnation ratio, the activation time, the interaction between impregnation ratio and activation time and the quadratic term of activation time have a positive impact on methyl violet removal. However, the other terms showed a negative effect. The linear term of impregnation ratio and the quadratic term of impregnation ratio have the greatest effect on the methyl violet removal with an *F*-value of 521.29 and 131.75, respectively, followed by linear term of activation time, the interaction between activation temperature-activation time, quadratic term of activation time and interaction between impregnation ratio-activation time with *F*-value of 9.98, 8.25, 7.89 and 5.4, respectively.

The most significant interactions were the interaction between activation temperature and activation time and the interaction between impregnation ratio and activation time. It was observed from the 3D response surface plot as shown in Fig. 4a that the methyl violet removal increasing with increasing the impregnation ratio and activation time, when the activation temperature is fixed at 450°C. Fig. 4b shows that when the activation time increases whatever the
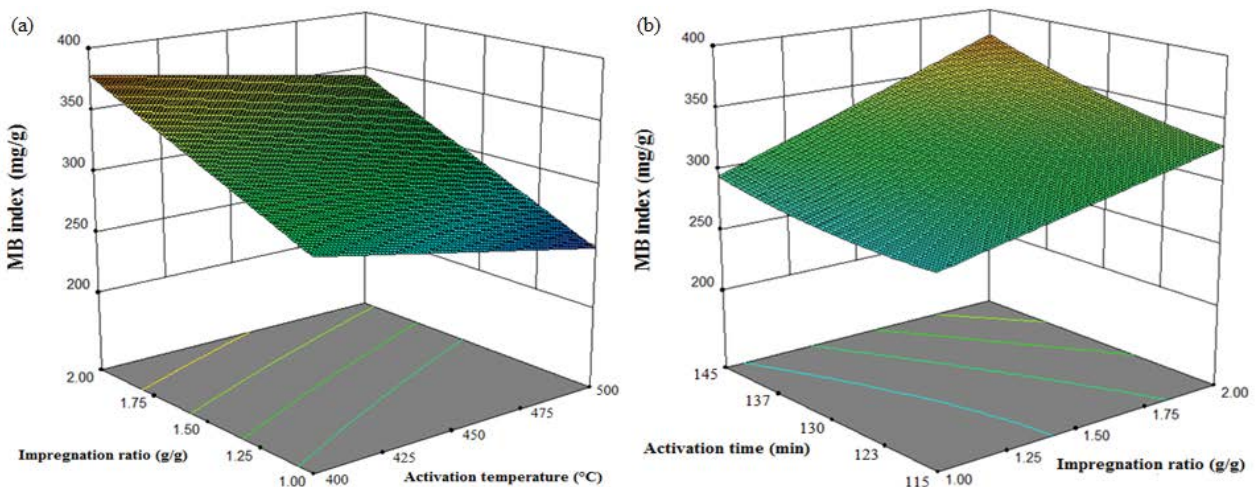
Fig. 2. Surface response plot for the methylene blue index: (a) interaction between impregnation ratio and activation temperature and (b) interaction between activation time and impregnation ratio.
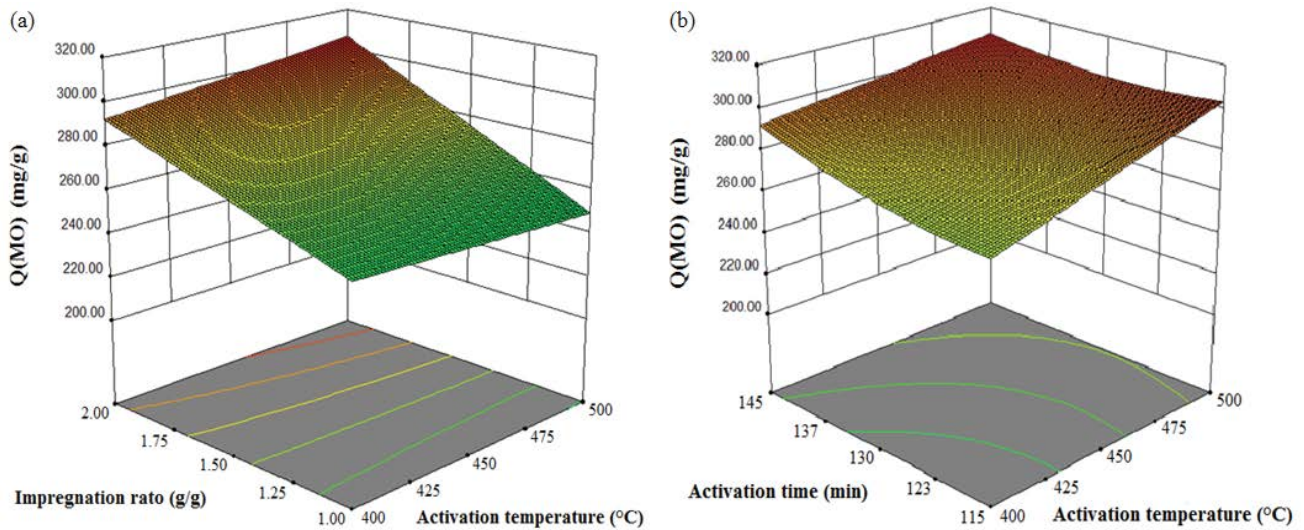
Fig. 3. Surface response plot for the methyl orange removal: (a) interaction between impregnation ratio and activation temperature and (b) interaction between activation time and activation temperature.
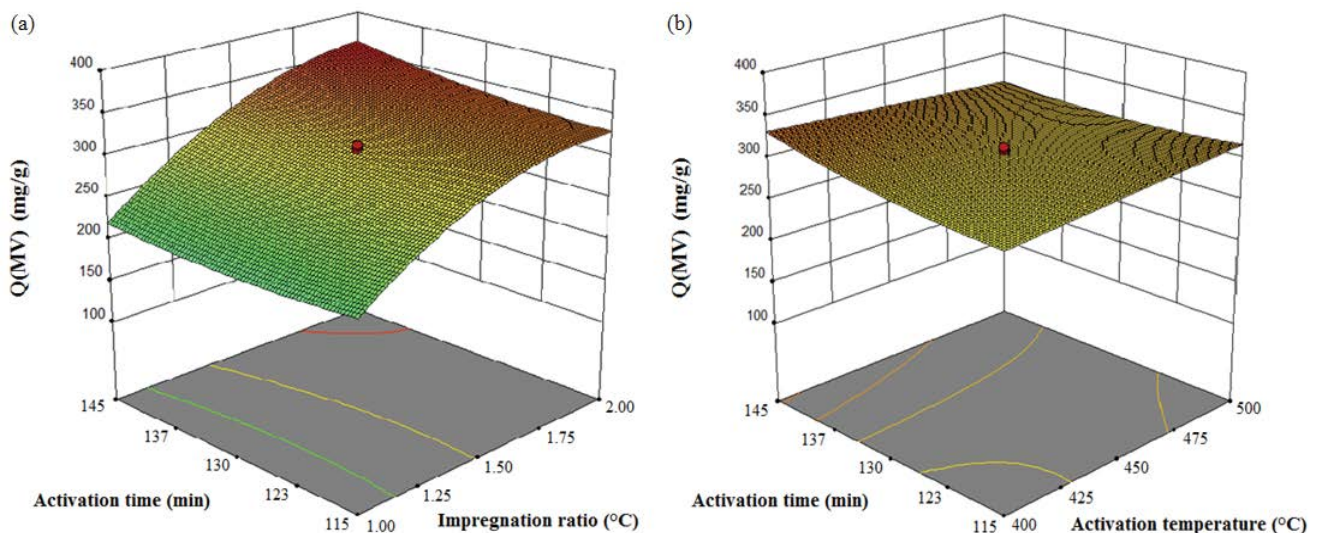
Fig. 4. Surface response plot for the methyl violet removal: (a) interaction between activation time and impregnation ratio and (b) interaction between activation time and activation temperature.

activation temperature, the methyl violet removal response increases.

3.2.5. Indigo carmine removal

Based on the ANOVA data for indigo carmine removal response, the most significant factors are activation temperature (A), impregnation ratio (B), activation time (C), interaction between activation temperature and activation time (AC), interaction between impregnation ratio and activation time (BC) and quadratic terms of impregnation ratio (B^2) and activation time (C^2) (Eq. (10)).

$$Y_5 = 156.20 + 12.59\,A + 18.70\,B + 8.66\,C - 6.33\,AC +$$
$$6.40\,BC + 14.21\,B^2 + 5.90\,C^2 \qquad (13)$$

The interaction between activation temperature and activation time has a negative impact on indigo carmine removal. However, the other terms showed a positive effect. The impregnation ratio, the quadratic term of impregnation ratio, the activation temperature and the activation time have the greatest effect on the indigo carmine removal with an F-value of 73.95, 45.52, 33.5 and 16.00, respectively.

The most significant interactions were the interaction between activation temperature and activation time and the interaction between impregnation ratio and activation time. Fig. 5a shows that the indigo carmine removal increased with increasing the activation temperature and activation time. Maximal indigo carmine removal is observed with an impregnation ratio of 1.5 g g⁻¹. Fig. 5b shows that when the impregnation ratio and activation time increase, the indigo
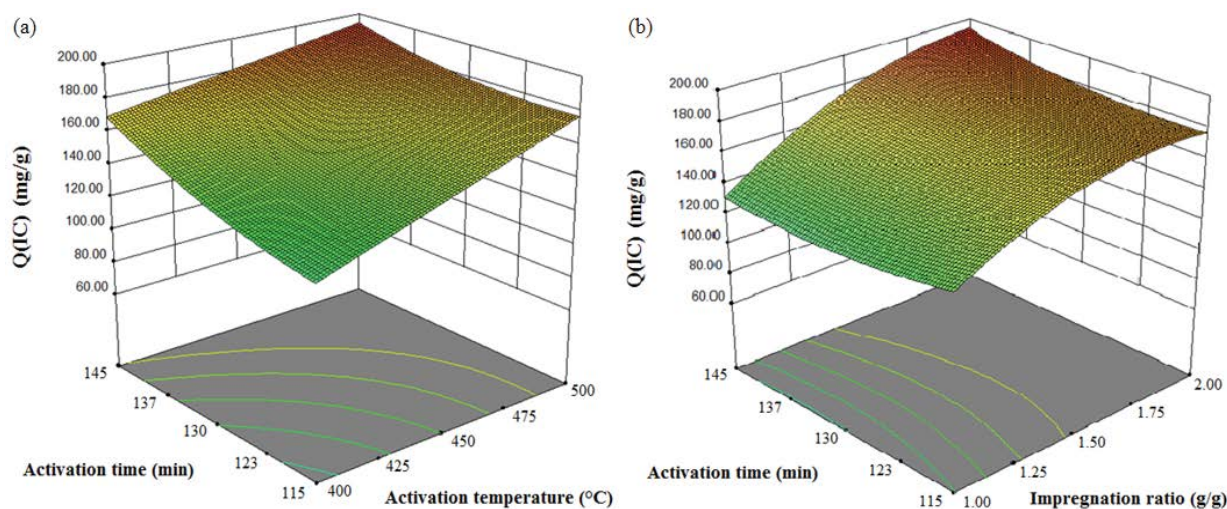
Fig. 5. Surface response plot for the indigo carmine removal: (a) interaction between activation time and activation temperature and (b) interaction between activation time and impregnation ration.

carmine removal response increases. The maximal indigo carmine removal was obtained at an activation temperature of 450°C.

3.3. Diagnostic model

The predicted and experimental results of five responses obtained at optimum conditions are listed in Table 6. As can be seen, the predicted values obtained were quite close to the experimental values, indicating that the models developed were successful in capturing the correlation between the responses and activated carbon preparation conditions. Therefore, the R^2 are in reasonable agreement with the R^2_{adj}. Besides, R^2 are greater than R^2_{adj}. In addition, The model *F*-value for the iodine number, methylene blue index, methyl orange, methyl violet and indigo carmine removal were 17.08, 11.36, 9.38, 98.79 and 27.26, respectively. These values implicate that models are significant.

3.4. Normal probability plot of residuals

The normal probability plot of the residuals is presented in Fig. 6. The normality of the data can be checked by plotting a normal probability plot of the residuals. If the data points on the plot fall fairly close to the straight line, then the data are normally distributed [46]. It appears that in the iodine number, methylene blue index and dyes removal responses, the data points were fairly close to the straight line and it indicates that the experiments come from a normally distributed population.

3.5. Optimization analysis

The objective of this study was to find the optimum process parameters that will produce activated carbons with high iodine number, high dyes removal, as well as high methylene blue index, but is very hard to optimize these responses under the same conditions. Therefore, the optimum conditions for three variables; activation temperature,

activation time and impregnation ratios, were obtained using numerical optimization feature of Design-Expert 10.0.0. From the experimental results, the maximum iodine number and methylene blue index obtained were 1,082.22, 397.54 mg g^{-1}, respectively. The best conditions for the removal of methyl violet were obtained by activated carbon sample activated at 400°C for 145 min with an impregnation ratio of 2 g g^{-1}. For methyl orange, the best conditions were activation temperature of 450°C, impregnation ratio of 1.5 g g^{-1} and activation time of 155 min. For indigo carmine, activation temperature of 500°C, impregnation ratio of 2 g g^{-1} and activation time of 145 min. Under these conditions, the maximum adsorption capacities were 358.67 mg g^{-1} for methyl violet, 305.88 mg g^{-1} for methyl orange and 196.06 mg g^{-1} for indigo carmine. In addition, it was observed that the experimental values obtained were in good agreement with the values predicted from the models, with relatively small errors between the predicted and the experimental values, which were only 0.01% for iodine number, methyl violet and indigo carmine removal responses, 0.04% for methyl orange removal and 0.02% for the methylene blue index responses.

3.6. Structural and textural properties of activated carbons

3.6.1. SEM observation of ACs

Fig. 7 shows the SEM images of the precursor and the selected activated carbons in various preparation conditions. Large and well-developed pores were clearly found on the surface of the activated carbons, compared with the original precursor. It can be seen from these images that the external surface of optimized ACs is full of pores of different sizes and shapes that have been developed during the chemical activation with different impregnation ratio of H$_3$PO$_4$ and heat treatment process. The production conditions strongly influence the porous structure of resulting activated carbon. Therefore, the pore diversity on the surface of each activated carbon prepared under optimal conditions could be the reason for the high sorption capacity.

Table 6
Factorial design matrix of three variables along with experimental and predicted responses for iodine number, methylene blue index, methyl orange, methyl violet and indigo carmine removal

Run	Iodine number			Methylene blue index			Methyl orange			Methyl violet			Indigo carmine		
	Actual	Predicted	Residual	Actual	Predicted	Residual	Actual	Predicted	Residual	Actual	Predicted	Residual	Actual	Predicted	Residual
1	1,019.39	1,015.16	4.24	307.21	303.68	3.53	270.35	265.24	5.11	311.93	306.61	5.32	159.32	156.20	3.12
2	1,015.20	1,015.16	0.05	302.36	303.68	-1.32	266.15	265.24	0.92	311.37	306.61	4.76	157.74	156.20	1.55
3	976.11	988.75	-12.64	258.17	270.59	-12.42	246.45	246.18	0.28	239.86	231.96	7.90	149.34	139.69	9.65
4	1,038.94	1,026.43	12.51	318.40	332.34	-13.94	305.88	288.60	17.29	349.66	342.34	7.32	188.97	187.44	1.53
5	1,004.03	1,003.88	0.15	313.26	308.77	4.49	260.66	267.53	-6.87	304.89	313.19	-8.30	149.87	158.31	-8.44
6	1,029.16	1,046.73	-17.57	313.50	294.92	18.58	253.55	255.57	-2.01	239.58	229.75	9.83	136.48	131.58	4.91
7	1,023.58	1,015.16	8.43	310.43	303.68	6.75	262.6	265.24	-2.64	313.34	306.61	6.73	154.07	156.20	-2.12
8	1,031.96	1,032.10	-0.14	284.51	322.63	-38.12	255.82	253.96	1.86	291.66	304.13	-12.47	128.61	135.03	-6.42
9	1,082.22	1,087.26	-5.04	317.48	329.51	-12.03	295.89	303.53	-7.64	338.68	341.22	-2.54	176.64	135.03	-0.11
10	1,001.24	999.70	1.54	293.25	281.70	11.56	246.77	233.71	13.06	217.90	208.32	9.58	117.32	135.03	3.09
11	1,012.41	1,015.16	-2.74	305.99	303.68	2.31	269.71	265.24	4.47	307.99	306.62	1.38	158.79	135.03	2.60
12	997.05	976.96	20.09	237.59	243.80	-6.21	205.43	225.61	-20.18	101.34	114.08	-12.74	76.64	135.03	-7.91
13	948.19	968.77	-20.58	245.16	249.25	-4.09	239.99	249.61	-9.62	206.64	212.00	-5.36	130.97	135.03	-0.48
14	1,045.92	1,039.14	6.78	397.54	378.57	18.97	287.47	292.56	-5.09	358.68	372.51	-13.83	164.57	135.03	-4.85
15	1,059.88	1,067.28	-7.40	339.57	344.57	-5.00	289.09	306.96	-17.88	352.47	354.76	-2.29	196.06	135.03	1.71
16	990.07	992.11	-2.04	339.59	328.95	10.65	270.67	270.71	-0.04	317.00	317.57	-0.57	131.49	135.03	5.28
17	1,011.01	1,015.16	-4.14	306.13	303.68	2.45	268.74	265.24	3.50	304.33	306.61	-2.28	160.37	135.03	4.17
18	1,048.71	1,053.35	-4.64	357.97	363.56	-5.59	303.94	304.86	-0.92	337.55	325.77	11.78	148.55	135.03	1.10
19	1,018.00	1,015.16	2.85	305.69	303.68	2.01	265.51	265.24	0.27	310.53	306.61	3.92	155.64	135.03	-0.55
20	1,066.86	1,046.54	20.32	302.15	284.74	17.41	302.65	276.52	26.13	300.95	309.08	-8.13	169.55	135.03	-7.81
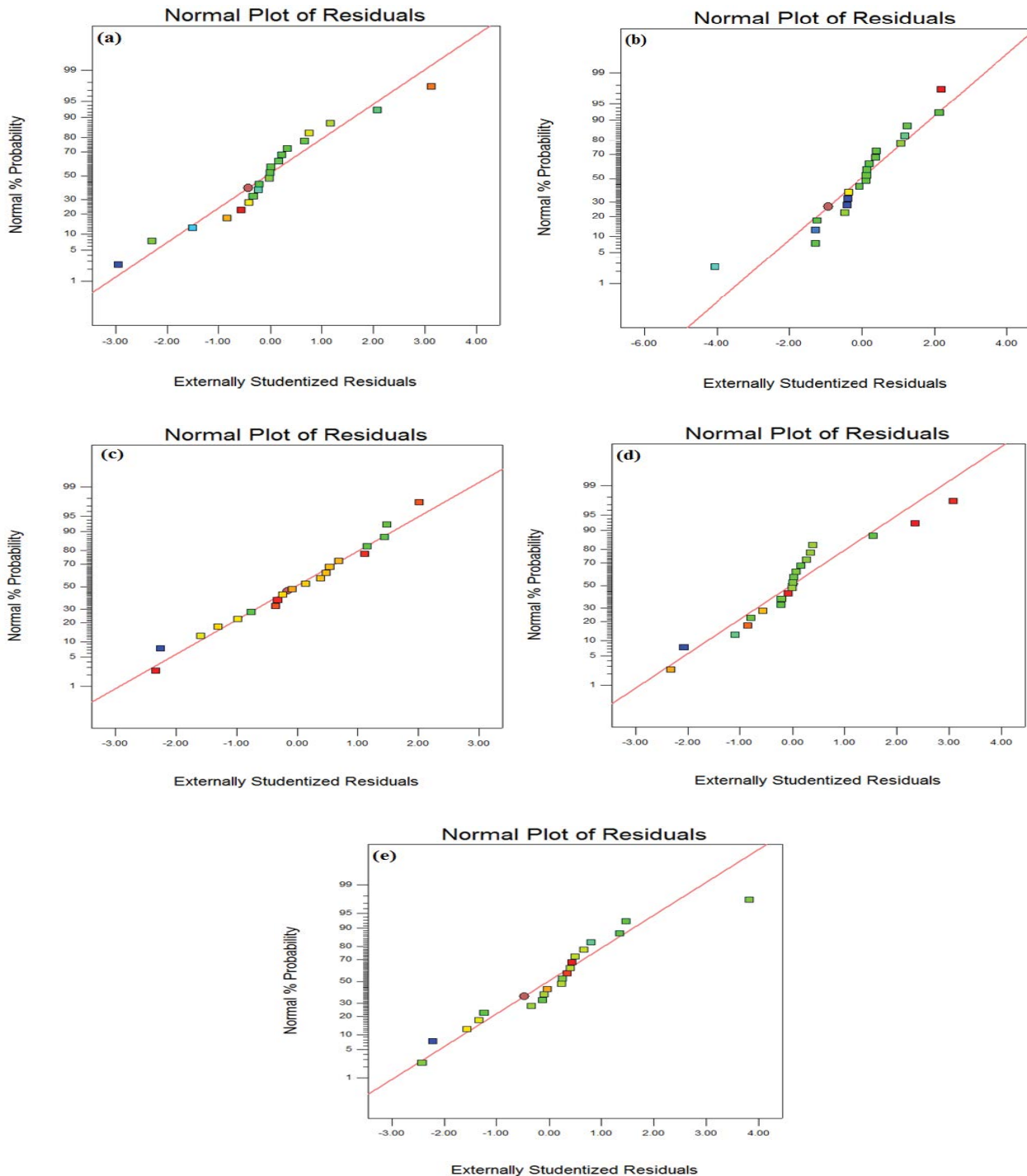
Fig. 6. Normal probability plots of residuals for the five responses: (a) iodine number, (b) methylene blue index, removal capacities (c) methyl violet, (d) methyl orange and (e) indigo carmine.

3.6.2. Energy dispersive X-ray analysis

The results of the EDX are given in Table 7. The raw material of TTS has higher carbon content, followed by oxygen, aluminum and low amounts of sodium, chlorine and potassium. After the impregnation by H_3PO_4, an increase of the carbon content by 24.17% and a decrease of the oxygen content by 19.49 for activated carbon prepared at 400°C for 145 min with an impregnation ratio of 2 g g^{-1}. For activated carbon prepared at 450°C for 155 min with an impregnation ratio of 1.5 g g^{-1}, there is an increase of the carbon content by 27.90% and a decrease of the oxygen content by 23.48%. For activated carbon prepared at 500°C for 145 min with an impregnation ratio of 2 g g^{-1}, there is an increase of the carbon
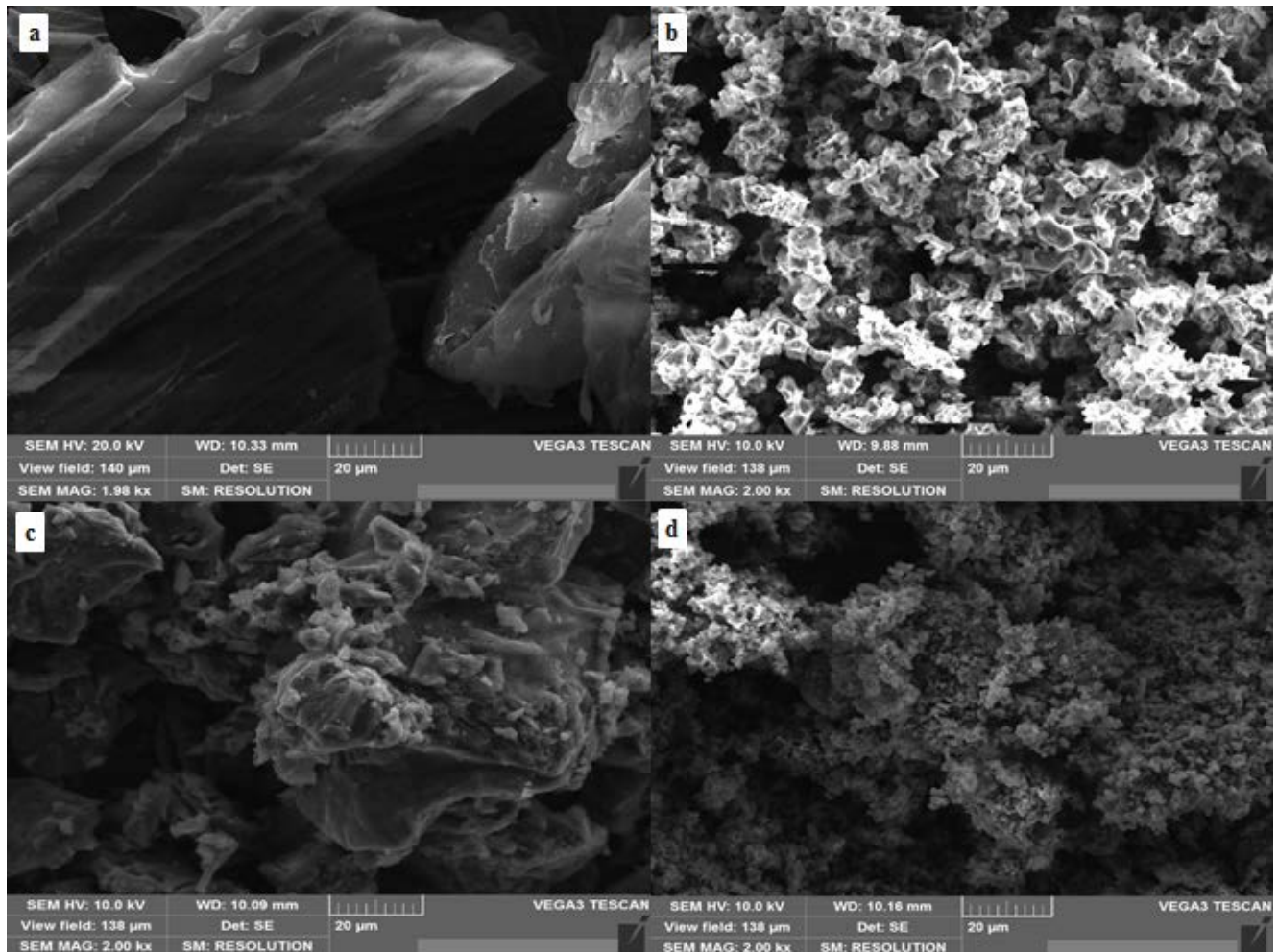
Fig. 7. SEM micrographs of: (a) precursor (TTS), (b) AC-500°C/145 min/2 g g⁻¹, (c) AC-400°C/145 min/2 g g⁻¹ and (d) AC-450°C/155 min/1.5 g g⁻¹.

content by 27.03% and a decrease of the oxygen content by 22.00%. These results indicate that the presence of carbon in significant quantity provided active surface for the attachments of the organic pollutants to the surface of the activated carbons.

3.6.3. X ray diffraction

The X-ray diffractograms of activated carbons prepared under optimal conditions are shown in Fig. 8. This figure shows an amorphous structure of all activated carbons with similar profiles. It is clearly seen that activated carbons possessed broad band at 24° and a weak band around 38°–45° assigning to the (002) and (100) crystal planes. The simple broad band at 24° may be attributed to the band of graphite. The weak intensity of the band around 38°–45° indicates the low crystallinity of graphite structure.

3.6.4. Boehm titration and pH of zero charge

The surface chemistry of carbon materials is basically determined by the acidity and basicity of their surface. Boehm titration is one of the most widely used methods to

Table 7
Percentage atomic of: (a) precursor (TTS), (b) AC-400°C/145 min/2 g g⁻¹, (c) AC-450°C/155 min/1.5 g g⁻¹ and (d) AC-500°C/145 min/2 g g⁻¹

Element	Atomic %			
	a	b	c	d
C	63.27	87.44	91.17	90.03
O	31.45	12.03	7.97	9.45
P	–	0.53	0.86	0.51
Al	4.62	–	–	–
Na	0.2	–	–	–
Cl	0.14	–	–	–
K	0.12	–	–	–

quantify acidic groups with different strengths on activated carbons. Table 8 presents the estimated chemical groups. The table shows that the surface of activated carbons is rich in acidic groups with a small amount of basic groups. Also, the quantity of phenolic and lactonic groups was
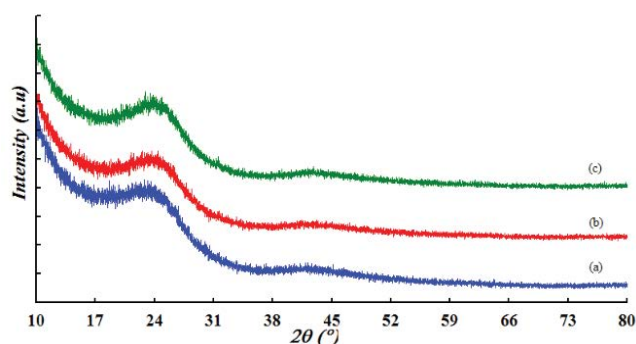
Fig. 8. XRD patterns of ACs: (curve a) 400°C/145 min/2 g g^{-1}, (curve b) 450°C/155 min/1.5 g g^{-1} and (curve c) 500°C/145 min/2 g g^{-1}.

Fig. 9. FTIR spectra of: (curve a) precursor (TTS), (curve b) AC-400°C/145 min/2 g g^{-1}, (curve c) AC-450°C/155 min/1.5 g g^{-1} and (curve d) AC-500°C/145 min/2 g g^{-1}.

significantly higher compared with the amount of carboxylic groups. Hence, the greater adsorption performance of cationic and anionic dyes of these activated carbons can be related to the availability of this type of functional groups. The pH$_{PZC}$ value is another characteristic which shows the acidic and basic properties of adsorbents beyond a definite pH value. It represents the pH value at the point where net charge on the surface of adsorbent is zero. Below pH$_{PZC}$, adsorbent has positive surface charge, while it is negative above pH$_{PZC}$. The pH$_{PZC}$ of the optimized activated carbons represented in Table 8. These values are in agreement with Boehm titration result, which show a dominance of acidic groups at the surface of the activated carbons.

3.6.5. Infrared spectroscopy

The FTIR spectra of the biomass TTS and the activated carbons were presented in Fig. 9. It can be seen from the figure that the surface groups of the activated carbons were different from the biomass. Some peaks were of low intensity or even disappeared in the prepared ACs compared with the raw TTS. This is due to the thermal degradation effect during the carbonization and activation processes which resulted in the destruction of some intermolecular bondings. For the precursor, there is a large band at 3,700–3,200 cm^{-1} attributed to the stretching vibration of hydrogen bended of the hydroxyl group linked in cellulose, lignin, adsorbed water and N–H stretching [47]. The bands at 2,935 cm^{-1} are due to the C–H stretching vibration. The stretching vibration band at 2,880 cm^{-1} is due to methoxy group (CH$_3$–O). The small band at 1,676 cm^{-1} is assigned to O–H bending. The spectra also indicate the bands at 1,615.95 cm^{-1} characteristic of asymmetric stretching of C=O
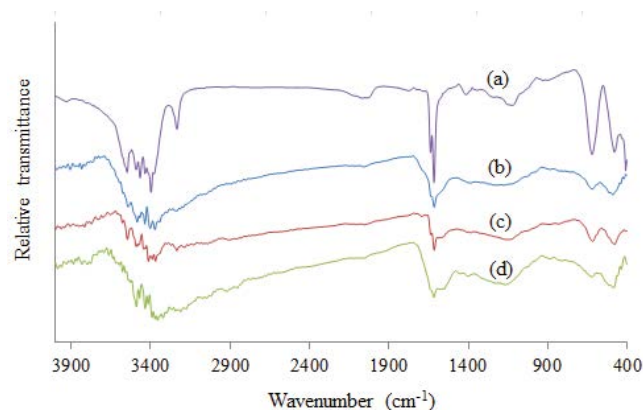
double bond vibrations of ketones, aldehydes, lactones or carboxyl groups [48].

The activated carbons present similar profiles with different band intensities. The band between 3,700 and 3,200 cm^{-1}, correspond to O–H stretching vibrations of the hydroxyl functional groups including hydrogen bonding, was of low intensity in ACs. This reduction in the peak intensity corresponds to the reduction in hydrogen bonding which may be due to the reaction between H$_3$PO$_4$ and precursor [49]. The band appearing on the spectrum between 1,700 and 1,500 cm^{-1} is attributed to vibrations of the C=O bonds. The shoulder at 970–900 cm^{-1} is attributed to chemical ionized bonding P$^+$–O [50] or the symmetric vibration in the P–O–P chains (polyphosphate) [51]. This band is an indication of the presence of phosphorus-oxygen compounds in the samples. It appears that activation of the samples impregnated with H$_3$PO$_4$ leads to decomposition of phosphoric compounds. Also, the shoulder at 640–600 cm^{-1} could correspond to vibration elongation of P–O–C (aliphatic), asymmetric elongation of P–O–C (aromatic), P–O stretching in >P=OOH, strain P–OH asymmetric stretching P–O–P in polyphosphates in complex phosphate-carbon.

3.6.6. Adsorption isotherms

According to CCD approach, the activated carbon having a highest potential ability to remove dyes was determined. In fact, the activated carbon activated at 400°C during 145 min with an impregnation ratio of 2 g g^{-1} was considered as optimized activated carbon for studying the isotherm models of

Table 8
Chemical groups on the surface of the ACs and their pH$_{PZC}$

Activated carbon	Functional groups (meq g^{-1})					pH$_{PZC}$
	Carboxylic	Lactonic	Phenolic	Total acid	Total basic	
CA-400°C/145 min/2 g g^{-1}	0.441	0.494	0.516	1.451	0.399	4.97
CA-450°C/155 min/1.5 g g^{-1}	0.445	0.498	0.532	1.475	0.406	4.58
CA-500°C/145 min/2 g g^{-1}	0.433	0.501	0.515	1.449	0.413	4.27

dyes adsorption. The adsorption isotherms were illustrated in Fig. 10. It was observed from this figure that the adsorption efficiency increases with increasing the initial concentration of dyes. The characteristics of these adsorption isotherms were described using Langmuir [52] and Freundlich [53] models.

Table 9 lists the fitting results of Langmuir and Freundlich isotherm models. The table shows that the correlation coefficients of Freundlich equation are lower than those of Langmuir model. The results from the fitting to Freundlich model show that the n values are greater than 1, which further support a favorable adsorption. Moreover, the maximum adsorption capacities obtained with the application of the Langmuir isotherm model are 439.08, 452.584, 288.610 and 188.252 mg g^{-1} for methylene blue, methyl violet, methyl orange and indigo carmine, respectively, onto the optimized
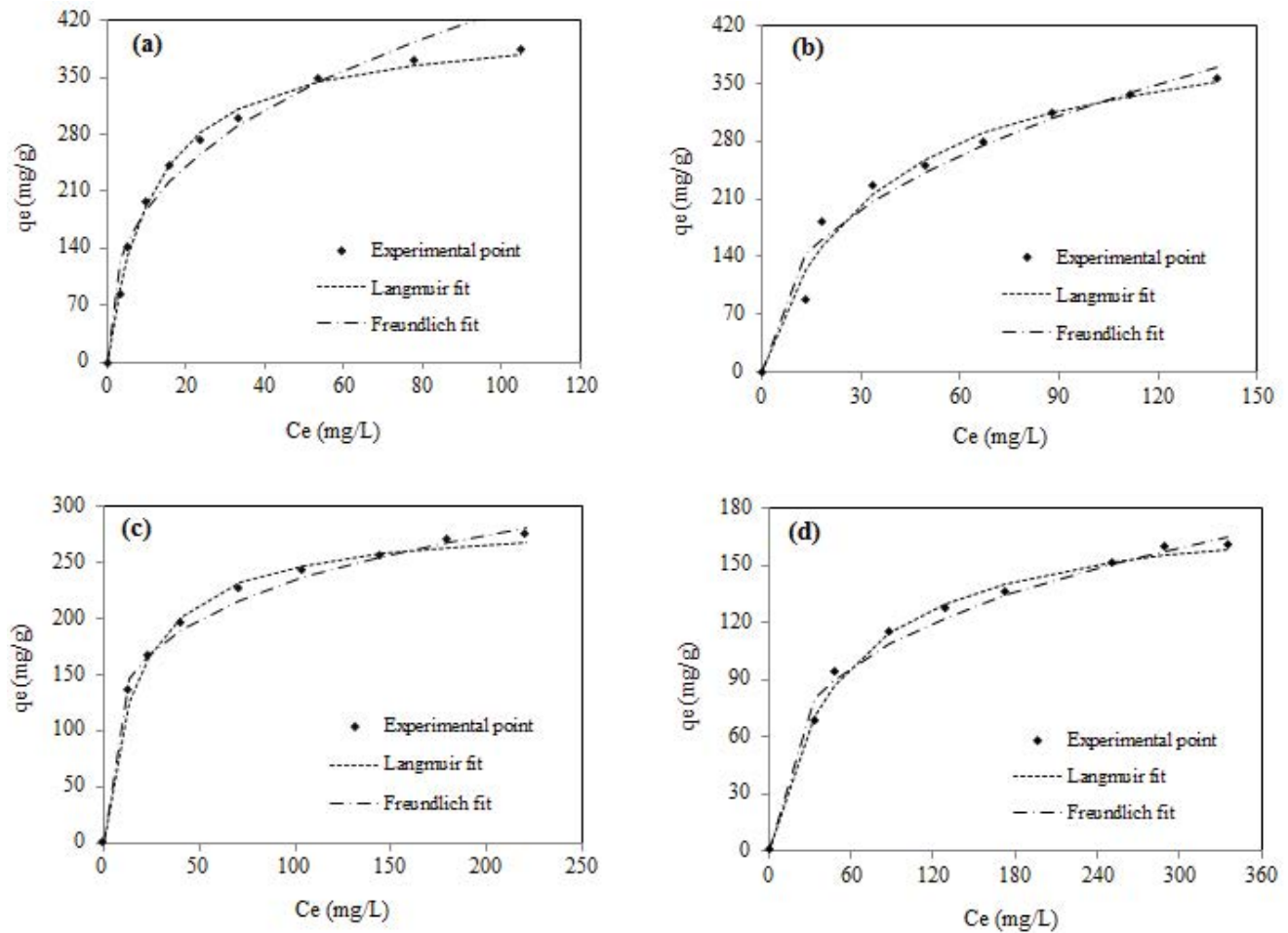
Fig. 10. Experimental points and nonlinear fitted curve isotherms of AC-400°C/145 min/2 g g^{-1}: removal of (a) methylene blue, (b) methyl violet, (c) methyl orange and (d) indigo carmine.

Table 9
Isotherm parameters for the adsorption of methylene blue, methyl violet, methyl orange and indigo carmine onto AC-400°C/145 min/2 g g^{-1}

Isotherm model	Parameters	Methylene blue	Methyl violet	Methyl orange	Indigo carmine
	q_m (mg g^{-1})	439.080	452.584	288.610	188.252
Langmuir	K_L (L mg^{-1})	0.082	0.026	0.060	0.017
	r^2	0.993	0.975	0.997	0.998
	n	2.992	2.266	4.190	2.977
Freundlich	K_F (mg$^{1-1/n}$ g^{-1} L$^{1/n}$)	88.628	42.012	78.131	23.515
	r^2	0.968	0.964	0.994	0.991

Table 10
Comparison of adsorption capacities of AC-400°C/145 min/2 g g^{-1} with literature

Activated carbon	Activating agent	Iodine number	Methylene blue	Methyl violet	Methyl orange	Indigo carmine	References
Activated coffee ground (CGAC)	HNO_3	–	–	–	558.00	–	[54]
Activated *Diplotaxis harra*	H_3PO_4	1,024.90	262.10	–	–	–	[55]
Activated *Glebionis coronaria* L.	H_3PO_4	794.58	161.92	–	–	–	[56]
Phragmites australis activated carbon (PAAC)	H_3PO_4	–	–	500.00	217.39	–	[57]
Activated *Camellia sinensis* leaves	H_3PO_4	1,050.90	322.70	–	–	–	[58]
Activated maize corncob (AMC)	H_3PO_4	–	271.19	–	–	–	[59]
Activated beetroot seeds	H_3PO_4	–	74.37	–	–	–	[60]
Activated apricot stones (ASAC)	$H_3PO_4 + HNO_3$	–	–	–	32.25	–	[61]
Activated Persian Mesquite Grain	H_3PO_4	–	–	–	66.30	–	[62]
Activated prickly pear peels (CarTunaQ)	H_3PO_4	–	–	–	–	294.10	[63]
Activated white sapote seeds (CarZapQ)	H_3PO_4	–	–	–	–	131.60	[63]
Activated broccoli stems (CarBrocQ)	H_3PO_4	–	–	–	–	312.50	[63]
Activated *Limonia acidissima* shell	H_3PO_4	1,056.10	–	–	–	–	[64]
Posidonia oceanica (L.) dead leaves	$ZnCl_2$	–	285.70	–	–	–	[65]
Activated *Glebionis coronaria* L.	KOH	571.18	284.04	–	–	–	[66]
Activated grapevine rhytidome (AC-51)	H_3PO_4 (microwave heating)	–	–	161.30	–	–	[67]
Commercial activated carbon	–	1,115.71	288.95	192.01	267.86	230.75	This study
Activated *Thapsia transtagana* stems (AC-400/2/145)	H_3PO_4	1,045.92	397.54	358.68	287.47	164.57	This study
Activated *Thapsia transtagana* stems (AC-450/1.5/155)	H_3PO_4	1,038.94	318.40	349.66	305.88	188.97	This study
Activated *Thapsia transtagana* stems (AC-500/2/145)	H_3PO_4	1,059.88	339.57	352.47	289.09	196.06	This study

AC. The maximum Langmuir adsorption capacities mentioned above were compared with previous studies on various activated carbons with different preparation conditions (Table 10). It could be seen that the experimental data in the present study are higher than the most prepared activated carbons used in literature.

4. Conclusion

This study examined the feasibility of preparing efficient activated carbons from *Thapsia transtagana* stems and their application in the removal of cationic and anionic dyes from aqueous solution. It was concluded that H_3PO_4 activation can successfully turn the TTS biomass into activated carbons with great performance. A CCD was used to optimize the production of activated carbons by studying the effects of the most important in the activation process (activation temperature, impregnation ratio and activation time). It was observed that the experimental values obtained were in good agreement with the values predicted from the models, with relatively small errors between the predicted and the experimental values. The best conditions for the removal of methyl violet were obtained by activated carbon sample activated at 400°C for 145 min with an impregnation ratio of 2 g g^{-1}. For methyl orange, the best conditions were activation temperature of 450°C, impregnation ratio of 1.5 g g^{-1} and activation time of 155 min. For indigo carmine, activation temperature of 500°C, impregnation ratio of 2 g g^{-1} and activation time of 145 min. Under these conditions, the maximum adsorption capacities were 358.68 mg g^{-1} for methyl violet, 305.88 mg g^{-1} for methyl orange and 196.06 mg g^{-1} for indigo carmine. The adsorption performance of the optimum activated carbon for cationic dyes was higher than a commercial activated carbon (267.86 mg g^{-1} for methyl orange and 192.01 mg g^{-1} for methyl violet), but lower for indigo carmine (230.75 mg g^{-1}). The mesoporosity of prepared activated carbon is higher than that of the commercial activated carbon (397.54 mg g^{-1} instead of 288.95 mg g^{-1} in methylene blue index). Whereas, the microporosity of prepared AC less than that of the commercial activated carbon (1,082.22 mg g^{-1} instead of 1,115.71 mg g^{-1} in iodine number).

References

[1] H. Métivier-Pignon, C. Faur-Brasquet, P. Le Cloirec, Adsorption of dyes onto activated carbon cloths: approach of adsorption mechanisms and coupling of ACC with ultrafiltration to treat coloured wastewaters, Sep. Purif. Technol., 31 (2003) 3–11.

[2] V.K. Gupta, Suhas, Application of low-cost adsorbents for dye removal – a review, J. Environ. Manage., 90 (2009) 2313–2342.

[3] R. Gong, Y. Ding, M. Li, C. Yang, H. Liu, Y. Sun, Utilization of powdered peanut hull as biosorbent for removal of anionic dyes from aqueous solution, Dyes Pigm., 64 (2005)187–192.

[4] A.M. Ferreira, J.A.P. Coutinho, A.M. Fernandes, M.G. Freire, Complete removal of textile dyes from aqueous media using ionic-liquid-based aqueous two-phase systems, Sep. Purif. Technol., 128 (2014) 58–66.

[5] G. Crini, Non-conventional low-cost adsorbents for dye removal: a review. Bioresour. Technol., 97 (2006) 1061–1085.

[6] G.Z. Kyzas, M. Kostoglou, Green adsorbents for wastewaters: a critical review, Materials, 7 (2014) 333–364.

[7] C. Duran, D. Ozdes, A. Gundogdu, H.B. Senturk, Kinetics and isotherm analysis of basic dyes adsorption onto almond shell (*Prunus dulcis*) as a low cost adsorbent, J. Chem. Eng. Data, 56 (2011) 2136–2147.

[8] B. Royer, N.F. Cardoso, E.C. Lima, J.C.P. Vaghetti, N.M. Simon, T. Calvete, R.C. Veses, Applications of Brazilian pine-fruit shell in natural and carbonized forms as adsorbents to removal of methylene blue from aqueous solutions—kinetic and equilibrium study, J. Hazard. Mater., 164 (2009) 1213–1222.

[9] M. Farnane, A. Elhalil, A. Machrouhi, F.Z. Mahjoubi, M. Sadiq, M. Abdennouri, S. Qourzal, H. Tounsadi, N. Barka, Enhanced adsorptive removal of cationic dyes from aqueous solution by chemically treated carob shells, Desal. Wat. Treat., 100 (2017) 204–213.

[10] M. El Ouardi, S. Qourzal, A. Assabbane, J. Douch, Adsorption studies of cationic and anionic dyes on synthetic ball clay, J. Appl. Surf. Interface, 1 (2017) 28–34.

[11] K. Kadirvelu, M. Kavipriya, C. Karthika, M. Radhika, N. Vennilamani, S. Pattabhi, Utilization of various agricultural wastes for activated carbon preparation and application for the removal of dyes and metal ions from aqueous solutions, Bioresour. Technol., 87 (2003) 129–132.

[12] A. Machrouhi, A. Elhalil, M. Farnane, F.Z. Mahjoubi, H. Tounsadi, M. Sadiq, M. Abdennouri, N. Barka, Adsorption behavior of methylene blue onto powdered Ziziphus lotus fruit peels and Avocado kernels seeds, J. Appl. Surf. Interface, 1 (2017) 49–56.

[13] A. Machrouhi, M. Farnane, A. Elhalil, M. Abdennouri, H. Tounsadi, S. Qourzal, N. Barka, Biosorption potential of *Thapsia transtagana* stems for the removal of dyes: kinetics, equilibrium, and thermodynamics, Desal. Wat. Treat., 126 (2018) 324–332.

[14] Z.N. Garba, A.A. Rahim, Adsorption of 4-chlorophenol onto optimum activated carbon from an agricultural waste, Int. J. Sci. Res., 4 (2015) 1931–1936.

[15] R.A. Shawabkeh, D.A. Rockstraw, R.K. Bhada, Copper and strontium adsorption by a novel carbon material manufactured from pecan shells, Carbon, 40 (2002) 781–786.

[16] T. Oymak, N. Eruygur, Effective and rapid removal of cationic and anionic dyes from aqueous solutions using *Elaeagnus angustifolia* L. fruits as a biosorbent, Desal. Wat. Treat., 138 (2019) 257–264.

[17] E. Köseoglu, C. Akmil-Başar, Preparation, structural evaluation and adsorptive properties of activated carbon from agricultural waste biomass, Adv. Powder Technol., 26 (2015) 811–818.

[18] B.H. Hameed, A.T.M. Din, A.L. Ahmad, Adsorption of methylene blue onto bamboo-based activated carbon: kinetics and equilibrium studies, J. Hazard. Mater., 141 (2007) 819–825.

[19] B.H. Hameed, A.L. Ahmad, K.N.A. Latiff, Adsorption of basic dye (methylene blue) onto activated carbon prepared from rattan sawdust, Dyes Pigm., 75 (2007) 143–149.

[20] F. Amaringo, A. Hormaza, Application of rice husk as an adsorbent for the simultaneous removal of a multicomponent system of dyes: evaluation of the equilibrium and kinetics of the process, Desal. Wat. Treat., 130 (2018) 200–211.

[21] Z.N. Garba, F.B.S. Shikin, A.R. Afidah, Valuation of activated carbon from waste tea for the removal of a basic dye from aqueous solution, J. Chem. Eng. Chem. Res., 2 (2015) 623–633.

[22] M. Danish, R. Hashim, M.N.M. Ibrahim, O. Sulaiman, Effect of acidic activating agents on surface area and surface functional groups of activated carbons produced from *Acacia mangium* wood, J. Anal. Appl. Pyrolysis, 104 (2013) 418–425.

[23] D. Cherik, K. Louhab, Preparation of microporous activated carbon from date stones by chemical activation using zinc chloride, Energy Sources Part A, 39 (2017) 1935–1941.

[24] M. Danish, T. Ahmad, W.N.A.W. Nadhari, M. Ahmad, W.A. Khanday, L. Ziyang, Z. Pin, Optimization of banana trunk-activated carbon production for methylene blue-contaminated water treatment, Appl. Water Sci., (2018), doi: 10.1007/s13201-018-0644-7.

[25] R.R. Gil, B. Ruiz, M.S. Lozano, E. Fuente, Influence of the pyrolysis step and the tanning process on KOH-activated carbons from biocollagenic wastes. Prospects as adsorbent for CO_2 capture, J. Anal. Appl. Pyrolysis, 110 (2014) 194–204.

[26] M. Farnane, A. Machrouhi, A. Elhalil, H. Tounsadi, M. Abdennouri, S. Qourzal, N. Barka, Process optimization of potassium

hydroxide activated carbon from carob shell biomass and heavy metals removal ability using Box–Behnken design, Desal. Wat. Treat., 133 (2018) 153–166.

[27] Ç. Kırbıyık, A.E. Pütün, E. Pütün, Equilibrium, kinetic, and thermodynamic studies of the adsorption of Fe(III) metal ions and 2,4-dichlorophenoxyacetic acid onto biomass-based activated carbon by $ZnCl_2$ activation, Surf. Interfaces, 8 (2017) 182–192.

[28] X. Liu, C. He, X. Yu, Y. Bai, L. Ye, B. Wang, L. Zhang, Net-like porous activated carbon materials from shrimp shell by solution-processed carbonization and H_3PO_4 activation for methylene blue adsorption, Powder Technol., 326 (2018) 181–189.

[29] I.I. Gurten, M. Ozmak, E. Yagmur, Z. Aktas, Preparation and characterisation of activated carbon from waste tea using K_2CO_3, Biomass Bioenergy, 37 (2012) 73–81.

[30] J. Antony, Design of Experiments for Engineers and Scientists, 1st ed., Butterworth-Heinemann, New York, 2003.

[31] J. Xu, L. Chen, H. Qu, Y. Jiao, J. Xie, G. Xing, Preparation and characterization of activated carbon from reedy grass leaves by chemical activation with H_3PO_4, Appl. Surf. Sci., 320 (2014) 674–680.

[32] M. Danish, T. Ahmad, A review on utilization of wood biomass as a sustainable precursor for activated carbon production and application, Renewable Sustainable Energy Rev., 87 (2018) 1–21.

[33] O. Ioannidou, A. Zabaniotou, Agricultural residues as precursors for activated carbon production—a review, Renewable Sustainable Energy Rev., 11 (2007) 1966–2005.

[34] M.T. Izquierdo, A.M. Yuso, B. Rubio, M.R. Pino, Conversion of almond shell to activated carbons: methodical study of the chemical activation based on an experimental design and relationship with their characteristics, Biomass Bioenergy, 35 (2011) 1235–1244.

[35] M. Danish, R. Hashim, M.N. Mohamad Ibrahim, O. Sulaiman, Optimized preparation for large surface area activated carbon from date (*Phoenix dactylifera* L.) stone Biomass, Biomass Bioenergy, 61 (2014) 167–178.

[36] S. Khodadoust, M. Hadjmohammadi, Determination of N-methylcarbamate insecticides in water samples using dispersive liquid–liquid microextraction and HPLC with the aid of experimental design and desirability function, Anal. Chim. Acta, 699 (2011) 113–119.

[37] M. Auta, B.H. Hameed, Optimized waste tea activated carbon for adsorption of methylene blue and acid blue 29 dyes using response surface methodology, Chem. Eng. J., 175 (2011) 233–243.

[38] Z.N. Garba, A.A. Rahim, Process optimization of $K_2C_2O_4$-activated carbon from *Prosopis africana* seed hulls using response surface methodology, J. Anal. Appl. Pyrolysis, 107 (2014) 306–312.

[39] S. Khodadoust, M. Ghaedi, Optimization of dispersive liquid–liquid microextraction with central composite design for preconcentration of chlordiazepoxide drug and its determination by HPLC-UV, J. Sep. Sci., 36 (2013) 1734–1742.

[40] A.A. Ahmad, B.H. Hameed, A.L. Ahmad, Removal of disperse dye from aqueous solution using waste-derived activated carbon: optimization study, J. Hazard. Mater., 170 (2009) 612–619.

[41] R. Kumar, R. Singh, N. Kumar, K. Bishnoi, N.R. Bishnoi, Response surface methodology approach for optimization of biosorption process for removal of Cr(VI) Ni(II) and Zn(II) ions by immobilized bacterial biomass sp. *Bacillus brevis*, Chem. Eng. J., 146 (2009) 401–407.

[42] C.G. Elliott, T.V. Colby, T.M. Kelly, H.G. Hicks, Charcoal lung: Bronchiolitis obliterans after aspiration of activated charcoal, Chest, 96 (1989) 672–674.

[43] American Society for Testing and Materials, Standard Test Method for Determination of Iodine Number of Activated Carbon, D4607, 94 (1999).

[44] H.P. Boehm, E. Diehl, W. Heck, R. Sappok, Surface oxides of carbon, Angew. Chem. Int. Ed., 3 (1964) 669–677.

[45] J.S. Noh, J.A. Schwarz, Estimation of the point of zero charge of simple oxides by mass titration, J. Colloid Interface Sci., 130 (1989) 157–164.

[46] M.K.B. Gratuito, T. Panyathanmaporn, R.-A. Chumnanklang, N.B. Sirinuntawittaya, A. Dutta, Production of activated carbon from coconut shell: optimization using response surface methodology, Bioresour. Technol., 99 (2008) 4887–4895.

[47] M.R.H. Mas Haris, K. Sathasivam, The removal of methyl red from aqueous solutions using banana pseudostem fibers, Am. J. Appl. Sci., 6 (2009) 1690–1700.

[48] M. Farnane, H. Tounsadi, R. Elmoubarki, F.Z. Mahjoubi, A. Elhalil, S. Saqrane, M. Abdennouri, S. Qourzal, N. Barka, Alkaline treated carob shells as sustainable biosorbent for clean recovery of heavy metals: kinetics, equilibrium, ions interference and process optimization, Ecol. Eng., 101 (2017) 9–20.

[49] F. Suárez-García, A. Martínez-Alonso, J. M.D. Tascón, Pyrolysis of apple pulp: chemical activation with phosphoric acid, J. Anal. Appl. Pyrolysis, 63 (2002) 283–301.

[50] D. Prahas, Y. Kartika, N. Indraswati, S. Ismadji, Activated carbon from jackfruit peel waste by H_3PO_4 chemical activation: pore structure and surface chemistry characterization, Chem. Eng. J., 140 (2008) 32–42.

[51] M. Danish, R. Hashim, M.N.M. Ibrahim, O. Sulaiman, Effect of acidic activating agents on surface area and surface functional groups of activated carbons produced from *Acacia mangium* wood, J. Anal. Appl. Pyrolysis, 104 (2013) 418–425.

[52] I. Langmuir, The constitution and fundamental properties of solids and liquids. Part I. Solids, J. Am. Chem. Soc., 38 (1916) 2221–2295.

[53] H. Freundlich, W. Heller, The Adsorption of *cis*- and *trans*-Azobenzene, J. Am. Chem. Soc., 61 (1939) 2228–2230.

[54] S. Rattanapan, J. Srikram, P. Kongsune, Adsorption of methyl orange on coffee grounds activated carbon, Energy Procedia, 138 (2017) 949–954.

[55] H. Tounsadi, A. Khalidi, M. Abdennouri, N. Barka, Activated carbon from *Diplotaxis Harra* biomass: optimization of preparation conditions and heavy metal removal, J. Taiwan Inst. Chem. Eng., 59 (2016) 348–358.

[56] H. Tounsadi, A. Khalidi, A. Machrouhi, M. Farnane, R. Elmoubarki, A. Elhalil, M. Sadiq, N. Barka, Highly efficient activated carbon from *Glebionis coronaria* L. biomass: optimization of preparation conditions and heavy metals removal using experimental design approach, J. Environ. Chem. Eng., 4 (2016) 4549–4564.

[57] S. Chen, J. Zhang, C. Zhang, Q. Yue, Y. Li, C. Li, Equilibrium and kinetic studies of methyl orange and methyl violet adsorption on activated carbon derived from *Phragmites australis*, Desalination, 252 (2010) 149–156.

[58] T. Mahmood, R. Ali, A. Naeem, M. Hamayun, M. Aslam, Potential of used *Camellia sinensis* leaves as precursor for activated carbon preparation by chemical activation with H_3PO_4; optimization using response surface methodology, Process Saf. Environ. Prot., 109 (2017) 548–563.

[59] M. Farnane, H. Tounsadi, A. Machrouhi, A. Elhalil, F.Z. Mahjoubi, M. Sadiq, M. Abdennouri, S. Qourzal, N. Barka, Dye removal from aqueous solution by raw maize corncob and H_3PO_4 activated maize corncob, J. Water Reuse Desal., 8 (2017) 214–224.

[60] A. Machrouhi, M. Farnane, A. Elhalil, R. Elmoubarki, M. Abdennouri, S. Qourzal, H. Tounsadi, N. Barka, Effectiveness of beetroot seeds and H_3PO_4 activated beetroot seeds for the removal of dyes from aqueous solutions, J. Water Reuse Desal., 8 (2018) 522–531.

[61] C. Djilani, R. Zaghdoudi, F. Djazi, B. Bouchekima, A. Lallam, A. Modarressi, M. Rogalski, Adsorption of dyes on activated carbon prepared from apricot stones and commercial activated carbon, J. Taiwan Inst. Chem. Eng., 53 (2015) 112–121.

[62] E.G. Lemraski, S. Sharafinia, M. Alimohammadi, New activated carbon from persian mesquite grain as an excellent adsorbent, Phys. Chem. Res., 5 (2017) 81–98.

[63] A.-A. Peláez-Cid, A.-M. Herrera-González, M. Salazar-Villanueva, A. Bautista-Hernández, Elimination of textile dyes using activated carbons prepared from vegetable residues and their characterization, J. Environ. Manage., 181 (2016) 269–278.

[64] S. Das, S. Mishra, Box-Behnken statistical design to optimize preparation of activated carbon from *Limonia acidissima* shell with desirability approach, J. Environ. Chem. Eng., 5 (2017) 588–600.

[65] M.U. Dural, L. Cavas, S.K. Papageorgiou, F.K. Katsaros, Methylene blue adsorption on activated carbon prepared from *Posidonia oceanica* (L.) dead leaves: kinetics and equilibrium studies, Chem. Eng. J., 168 (2011) 77–85.

[66] H. Tounsadi, A. Khalidi, M. Farnane, M. Abdennouri, N. Barka, Experimental design for the optimization of preparation conditions of highly efficient activated carbon from *Glebionis coronaria* L. and heavy metals removal ability, Process Saf. Environ. Prot., 102 (2016) 710–723.

[67] M. Hejazifar, S. Azizian, H. Sarikhani, Q. Li, D. Zhao, Microwave assisted preparation of efficient activated carbon from grapevine rhytidome for the removal of methyl violet from aqueous solution, J. Anal. Appl. Pyrolysis, 92 (2011) 258–266.